Simulation-Supported Analysis of Calendering Impacts on the Performance of Lithium-Ion-Batteries

Georg Lenze,[a,b] Fridolin Röder,[a,b] Henrike Bockholt,[b,c] Wolfgang Haselrieder,[b,c] Arno Kwade,[b,c] and Ulrike Krewer[a,b,z]

[a]*Institute of Energy and Process Systems Engineering, TU Braunschweig, 38106 Braunschweig, Germany*
[b]*Battery LabFactory Braunschweig, 38106 Braunschweig, Germany*
[c]*Institute for Particle Technology, TU Braunschweig, 38106 Braunschweig, Germany*

A combination of experimental and model based analysis was performed to investigate calendering impacts on the performance of lithium-ion-batteries. When discharging, not only geometric parameters, such as electrode thicknesses and porosities are affecting performance. Calendering also impacts on other parameters, such as the effective ionic conductivity within the electrolyte, the effective electronic conductivity of solid active material and the effective solid-liquid interfacial area. The simulation supported method is shown to complement experimental analysis to understand correlations between calendering and these parameters; it enables to identify cell internal parameters which are hard to measure and to analyze how the lithium transport is affected. In experiments, cells containing non-calendered cathodes performed significantly worse than ones with 22%-calendered cathodes. Simulation indicated that this losses consist mainly of a deterioration of effective electronic conductivity leading to overpotentials close to the separator. Minor contributions to the losses in non-calendered cathodes caused by the geometric compaction and a reduction of effective solid-liquid interfacial area were found as well, whereas the impact of effective ionic conductivity turned out to be only insignificantly small.

Calendering of electrodes is an important step within the manufacturing process of lithium-ion-batteries as it affects energy density significantly.[1] An increase in energy density is crucial to achieve larger driving ranges for electric vehicles and thus to make them competitive on the market. Aim of this work is to establish an advanced model based method for the analysis of calendering impacts which gives additional insights into cell internal electrochemical correlations. Most studies about calendering impacts on battery electrodes are of experimental nature.[1–3] These investigations present mechanical and electrochemical characterization results of industrially produced and readily usable electrode samples. Usually mercury (Hg) porosimetry, scanning electron microscopy (SEM), electrochemical impedance spectroscopy (EIS), C-Rate, and cycling tests are performed. These methods are helpful to understand how calendering affects the geometric and mechanical properties of particle-pore networks within electrodes. However, evaluation of correlations between structural changes and battery performance is rather phenomenological and empirical so that knowledge gained is limited. EIS measurements are commonly used for correlation between structural changes and performance determining physico-chemical processes and constants, such as electronic conductivity within the electrode;[4,5] to investigate calendering impacts on the aging behavior cycling experiments have been used [6]. However, it is still difficult to understand calendering impacts on performance entirely, as calendering affects several parameters simultaneously, making evaluations complex. Additional tools for analysis can improve this understanding and enable knowledge-driven optimization of manufacturing parameters. Physico-chemical battery models enable to simulate battery performance as a function of structural parameters, such as electrode thickness and porosity,[7] as well as of parameters like solid-liquid interfacial area, electronic and ionic conductivities, which may be affected by calendering as well.[8] Furthermore, not only the resulting battery performance but underlying processes like lithium (Li) transport within electrolyte, electrodes and active material particles can be studied.[9] These features make simulation a promising complementary tool to experimental investigations for understanding calendering impacts in Li-ion-batteries and the related structure-performance correlations. We see simulation therefore as essential to achieve an optimized battery production. Approaches of simulating structure-performance correlations in lithium-ion-batteries can be found in literature; they are rather theoretical, as they primarily focus to improve modeling from mathematical point of view.[10,11] Thorat et al. present a method where experimental and model-supported analysis are combined to determine electrode tortuosities and resulting effective resistances within liquid phases of porous cathode materials in half cells.[12] This contribution may be a useful foundation for experimental and model-supported investigation of full cells. In general, several works present particular variations of physico-chemical battery models[9,13,14] which are based on porous electrode and concentrated solution theory.[15,16] A gap between theory oriented modeling and behavior of real battery cells is apparent, though, as parameterization of models requires significant experimental experience and effort on the analyzed cell. Most presented model approaches therefore either take a part or even all of the parameters from literature or estimate them. Recently, Ecker et al. presented studies where parameterization based on exclusively experimentally determined values in real battery cells was focused.[17,18]

Aim of this work is to improve knowledge about calendering impacts on battery cell performance by combining well established experimental methods with physico-chemical simulation. Furthermore, we focus on an optimal parameterization strategy for analyzing cathodic calendering impacts and for simulating the particular behaviors of battery cells manufactured inhouse for this study. These produced lithium-ion-batteries were pouch cells with two different calendering configurations. Both configurations were assembled with C_6 (graphite) anodes and $Li(Ni_{1/3}Mn_{1/3}Co_{1/3})O_2$ (NMC) cathodes. However, while anode active material layers were calendered to a compression degree of 10% of their original thickness for all produced cells, cathodes were either non-calendered or calendered to a compression degree of 22%.

Various experiments, being namely C-Rate test, measurement of electronic conductivity for battery performance characterization and other measurements for model parameterization were carried out for both calendering configurations. Thus two parameter sets were determined. After experimental analysis and model parameterization, simulation studies are presented and discussed within the context of experimental results in order to evaluate calendering impacts on Li transport within the cell and on battery performance. In Figure 1 all steps of simulation supported analysis are summarized.

Experimental

Battery cells.—Individual electrodes were manufactured and assembled at the Battery LabFactory Braunschweig as pouch full cells

[z]E-mail: u.krewer@tu-braunschweig.de

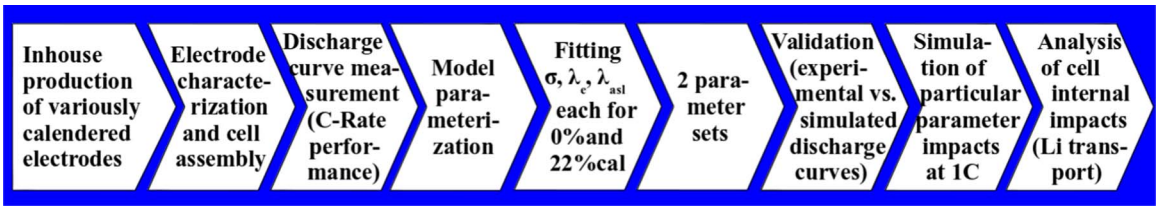

Figure 1. Methodology of simulation supported analysis.

(electrode surface area $A = 24.95$ cm^2). The inhouse production enables for targeted variation of particular manufacturing parameters, being namely the level of cathode compaction by calendering within this work. A CELGARD2320 separator and a solution consisting of 3:7 EC:DEC, 1 M $LiPF_6$ was used as electrolyte. Two cell configurations were produced for investigation:

1) C_6, 10% calendered vs. $Li(Ni_{1/3}Mn_{1/3}Co_{1/3})O_2$, non-calendered

2) C_6, 10% calendered vs. $Li(Ni_{1/3}Mn_{1/3}Co_{1/3})O_2$, 22% calendered.

Both types of cells contain electrode material loadings, $\varpi_a = 4.19$ mg/cm^2 and $\varpi_c = 9.63$ mg/cm^2, accordingly same cell theoretical capacities were expected. The solid electrode material compositions contained mass fractions of inactive additives, binder $\zeta^a_{binder} = 0.05$ and conductive carbon black $\zeta^a_{carbonblack} = 0.05$ within the anode and $\zeta^c_{binder} = 0.04$, $\zeta^c_{carbonblack} = 0.04$ within the cathodes, respectively.

Electrochemical characterization.—The cells were formated by constant current charging and discharging twice at a 0.05 C-Rate where the related currents were calculated to $I_{formation} = 1.7$ mA based on theoretical capacities given in the active material data sheets. Real cell capacities were then defined as the discharge capacities achieved during the second formation cycle. These were used for calculation of currents to be applied in the C-Rate tests; exemplarily the respective 1 C currents are given with $I^{0\%cal} = 31.74$ mA and $I^{22\%cal} = 32.06$ mA. For evaluation of cell performance, in the C-Rate test discharge curves at 0.2 C, 0.5 C, 1 C and 2 C were measured within a range of cut-off-voltages 2.9 V and 4.2 V, where the cycling was performed by constant current operation and recharging at 0.2 C after each discharge. To determine cathode open circuit potentials (OCP) as a function of state of charge for model parameterization, discharge measurements at a 1/50 C-Rate were performed. Electrode samples ($A_{EL-Cell} = 2.54$ cm^2) were assembled in an EL-Cell ECC-Ref setup with an EL-Cell glass fiber separator ECC1-01-0012-C/X and the same electrolyte as the one used in pouch cells. Due to the low C-Rate it was assumed that kinetic losses were negligible; consequently effects from different separators used in pouch cells and EL-Cells were neglected. Half cell potentials were measured by application of a Li wire as reference electrode. OCP of an electrode is assumed to be only dependent on material composition; therefore the experiment was not repeated for both cathode calendering configurations but only performed on cells containing 22%-calendered cathodes. OCP of the anode was taken from literature,[19] because it was assumed to be generally valid for graphite. As opposed to this NMC was regarded as a more particular material where shares of the included metals may fluctuate among various manufacturers which would affect OCP; therefore it was determined experimentally for the cathode used in this study.

Thicknesses and electronic conductivities of electrodes.—Electrode thicknesses were measured using a tactile gauge with an accuracy of ± 1 µm (Mitutoyo, Digimatic ID-C). For experimental determination of effective electronic conductivities σ_{eff} we took five samples of anodes, non-calendered and 22%-calendered cathodes respectively, circular with a geometric area $A_{sample} = 1.13$ cm^2. For these experiments, we used a Zwick Z010 where a sample is placed between two stamps which are then pressed together applying a force of 40 N. A current of $I = 10$ mA is passed through the sample and the resulting voltage drop is measured to determine an absolute value for electronic resistance R_Ω of electrode including current collector. Electronic conductivity can then be calculated by:

$$\sigma_{eff} = \frac{A_{sample}}{R_\Omega \cdot d_{sample}} \quad [1]$$

Mathematical Model

For simulation-supported battery analysis, we used a pseudo 2-dimensional (P2D) physico-chemical battery model based on the approaches introduced by Newman, Doyle et al.;[15,16] this approach can be used in several individually modified versions.[9,13,14] For our analysis of calendering impacts, we implemented a model based on equations given by Legrand et al.[13] The P2D model approach is state of the art in battery modeling and validated to be able to reproduce cell performance,[9] where P2D describes spatial discretization perpendicular through electrodes-separator layers and radial discretization within active material particles, respectively. (Figure 2).

Lithium transport.—Lithium diffusion within the solid active material particles during battery discharge is implemented into the model using Fick's law:

$$\frac{\partial c_s(r)}{\partial t} = \frac{1}{r^2} \cdot \frac{\partial}{\partial r}\left(D_s \cdot r^2 \cdot \frac{\partial c_s(r)}{\partial r}\right) \quad [2]$$

discretized over the radial coordinate r with Li concentration c_s and the boundary conditions for the solid diffusion equation at particle surface ($r = R_s$) and particle center ($r = 0$):

$$-D_s \cdot \frac{\partial c_s(0)}{\partial r} = 0 \quad [3]$$

and:

$$-D_s \cdot \frac{\partial c_s(R_p)}{\partial r} = \frac{j^{Li}}{a_{sl} \cdot F} \quad [4]$$

with j^{Li} as volume rate of Li^+ exchange current generation, where the theoretic solid-liquid interfacial area per volume unit a_{sl} is determined by the surface area of spherical active material particles:

$$a_{sl} = \frac{3 \cdot \varepsilon_s}{R_p} \quad [5]$$

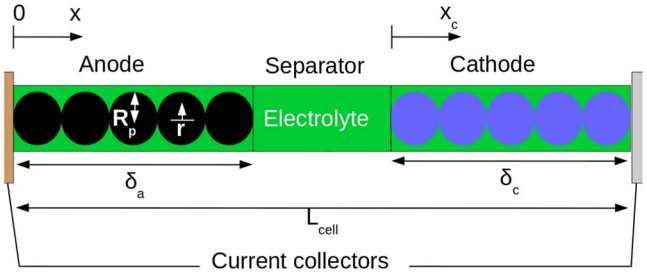

Figure 2. Discretization scheme of P2D battery model.

with R_p as particle radius and ε_s as solid active material fraction. Transport of Li salt $LiPF_6$ within the liquid electrolyte, is considered by the partial differential equation for diffusion:

$$\varepsilon \frac{\partial c_e(x)}{\partial t} = \frac{\partial}{\partial x} \cdot \left(D_e^{eff} \cdot \frac{\partial c_e(x)}{\partial x} \right) + (1 - t_+) \cdot \frac{j^{Li}(x)}{F} \quad [6]$$

with porosity ε and the boundary conditions:

$$- D_e^{eff} \cdot \frac{\partial c_e}{\partial x}(0) = 0 \quad [7]$$

$$- D_e^{eff} \cdot \frac{\partial c_e}{\partial x}(L_{cell}) = 0 \quad [8]$$

where coordinate x=0 denotes the boundary between anode and related current collector whereas the boundary between cathode and related current collector is located at x=L_{cell}. Within Equation 6 the effective liquid diffusion coefficient D_e^{eff} is of particular relevance as it is assumed to be affected by calendering. Therefore, within this work a modified version of the equation used in Ref. 13 was implemented:

$$D_e^{eff} = \frac{D_e \cdot \varepsilon}{\tau} \quad [9]$$

where the tortuosity τ is a fitting parameter to be adjusted in the model in order to achieve agreement between experimental and simulated discharge curves for both calendering configurations. Equation 9 depends on tortuosity τ and porosity ε which both are assumed to be affected by calendering.

Electronic and ionic conduction.—Electric potentials ϕ_s within the solid active material are described in the model by Ohm's Law:

$$J_s(x) = -\sigma_{s,eff} \cdot \frac{\partial \phi_s(x)}{\partial x} \quad [10]$$

$$\frac{\partial J_s(x)}{\partial x} = -(j^{Li}(x) + j^{DL}(x)) \quad [11]$$

with J_s as solid current density and $\sigma_{s,eff}$ as effective electronic conductivity. Related boundary conditions are:

$$J_s(0) = \frac{I_{cell}}{A_{cell}} \quad [12]$$

$$J_s(\delta_a) = 0 \quad [13]$$

$$J_s(L_{cell} - \delta_c) = 0 \quad [14]$$

$$J_s(L_{cell}) = \frac{I_{cell}}{A_{cell}} \quad [15]$$

Impacts of calendering on the effective electronic conductivity are assumed to occur, first because the solid active material fraction ε_s is increased by geometric compaction and second because the carbon black particle network is restructured which affects the electronic conductivity σ of the bulk. These correlations are stated by:

$$\sigma_{s,eff} = \sigma \cdot \varepsilon_s \quad [16]$$

The charge transport, including the electric potential ϕ_e in the electrolyte can be written as:

$$J_e(x) = -\kappa_{\mathrm{eff}}^{e}(x) \frac{\partial \phi_e(x)}{\partial x} - \kappa_{\mathrm{eff}}^{\mathrm{De}}(x) \frac{\partial ln(c_e(x))}{\partial x} \quad [17]$$

$$\frac{\partial J_e(x)}{\partial x} = +(j^{Li}(x) + j^{DL}(x)) \quad [18]$$

with $J_e(x)$ as electrolyte current density, c_e as $LiPF_6$ concentration, j^{Li} as volume rate of exchange current generation and j^{DL} as volume rate of double layer current generation. Furthermore κ_{eff}^{e} as effective ionic conductivity and κ_{eff}^{De} as effective diffusional ionic conductivity within the electrolyte are included; a detailed discussion on the derivation of Equation 17 can be found in the paper of Legrand et al.[13] Within this work the equation of effective ionic conductivity was modified in order to account for the electrode tortuosity τ:

$$\kappa_{eff}^{e} = \frac{\kappa \cdot \varepsilon}{\tau} \quad [19]$$

where the ionic conductivity κ of the used electrolyte as a function of $LiPF_6$ concentration c_e and temperature T, based on the measurement by Moosbauer [24] was approached by the polynomial:

$$\begin{aligned} \kappa(x) = {} & B_0 + B_1 \cdot T + B_2 \cdot c_e(x) + B_3 \cdot T^2 + B_4 \cdot T \cdot c_e(x) \\ & + B_5 \cdot c_e^2(x) + B_6 \cdot T^2 \cdot c_e(x) + B_7 \cdot T \cdot c_e^2(x) + B_8 \cdot c_e^3(x) \\ & + B_9 \cdot T^2 \cdot c_e^2(x) + B_{10} \cdot T \cdot c_e^3(x) + B_{11} \cdot c_e^4(x) \end{aligned} \quad [20]$$

Associated coefficients $B_0 - B_{11}$ are listed in Table A1 in the appendix. The effective diffusional ionic conductivity κ_{eff}^{De} is given by:

$$\kappa_{eff}^{De} = \kappa_{eff}^{e} \cdot \frac{2 \cdot R \cdot T \cdot (t_+ - 1)}{F} \quad [21]$$

Boundary conditions are:

$$\frac{\partial \phi_e(x)}{\partial x}(0) = 0 \quad [22]$$

$$\phi_e(L_{cell}) = 0 \quad [23]$$

Electrochemical reaction kinetics and cell voltage.—The Butler-Volmer equation was implemented to describe the charge transfer reaction as:

$$j^{Li}(x) = a_{sl} \cdot \lambda_{asl} \cdot j_0 \cdot \left[\exp\left(\alpha_o \frac{F\eta(x)}{RT} \right) - \exp(-\alpha_r \frac{F\eta(x)}{RT} \right) \Bigg] \quad [24]$$

with the transfer coefficients for oxidation and reduction α_o and α_r, where λ_{asl} is a calendering dependent factor which takes into account the effective share of solid-liquid interfacial area which participates in reaction. It is assumed that structural changes within the electrode induced by calendering may affect the effectively utilized interfacial area:

$$a_{sl}^{eff} = a_{sl} \cdot \lambda_{asl} \quad [25]$$

A concentration dependent approach[19] was applied to implement the exchange current density:

$$j_0 = k \cdot F \cdot c_e^{\alpha_o} (c_{max,s} - c_s)^{\alpha_o} \cdot c_s^{\alpha_r} \quad [26]$$

where k is the chemical reaction rate constant. The overpotentials for anode and cathode respectively are calculated by the equation:

$$\eta(x) = \phi_s(x) - \phi_e(x) - U(x) \quad [27]$$

where $U(x)$ denotes the open circuit potential (OCP) which is characteristic for the respective chemical composition of electrodes and depends on the concentration of intercalated Li within the electrodes, which changes during battery discharge. Charge balance is included at the electrochemical double layer with C_{DL} as the double layer capacitance:

$$j^{DL}(x) = a_{sl} \cdot C_{DL} \cdot \frac{\partial(\phi_s(x) - \phi_e(x))}{\partial t} \quad [28]$$

Finally, battery cell voltage can be calculated by:

$$E_{cell} = \phi_s(L_{cell}) - \phi_s(0) \quad [29]$$

Parameterization

Electrode layer thicknesses δ were measured for anodes and cathodes respectively and the determined values were used to calculate component mass fractions of active material and additives in the electrodes where the latter is a compound of carbon black and PVDF as binder:

$$\varepsilon^{s}_{act} = \frac{\varpi}{\delta} \cdot \frac{\zeta_{act}}{\rho_{act}} \quad [30]$$

$$\varepsilon^{s}_{add} = \frac{\varpi}{\delta} \cdot \frac{\zeta_{add}}{\rho_{add}} \quad [31]$$

with electrode material loadings ϖ and mass fractions ζ which were given by electrode manufacturing formulation and densities ρ taken from Refs. 21–23. Electrode porosities can be calculated by

$$\varepsilon = 1 - \varepsilon^{s}_{act} - \varepsilon^{s}_{add} \quad [32]$$

Thickness and porosity of the anode were kept constant during simulation studies within this work, whereas the values for cathodes were calculated for the non-calendered and for the 22%-calendered case respectively, as electrode geometry is obviously affected by compaction. As a small share of calendering induced deformation is elastic, measured thickness of the calendered cathode turned out to be slightly thicker than the adjusted thickness reduction of 22% would imply. All other parameters will be categorized into independent and dependent of calendering within following subsections.

Parameters independent of calendering.—Maximum Li concentrations c^{max} within the respective active materials of anode and cathode were determined by the active materials' chemical structural formulae in the fully lithiated states Li_1C_6 and $Li_1(Ni_{1/3}Mn_{1/3}Co_{1/3})O_2$ and corresponding molecular masses M:

$$c^{max} = \frac{\zeta \cdot \varpi \cdot A}{M \cdot \varepsilon^{s}_{act} \cdot V} \quad [33]$$

with geometric electrode areas and volumes A and V. Initial Li concentrations at 100% state of charge, c^0_a and c^0_c, were then calculated with respect to the battery's cycling balance since cell assembly using Faraday's law:

$$c_0 = \frac{C}{F \cdot \varepsilon^{s}_{act} \cdot V} \quad [34]$$

with the measured capacity C being shifted between cathode and anode during charging and discharging. The loss of lithium due to SEI formation comprises about 10% of Li amount being shifted to the anode during formation.[28] To consider this loss in the model c^0_a was after determination according to Equation 34 reduced by $0.1c^{max}_a$. Material specific open circuit potential (*OCP*) curves being dependent on inserted amount of Li, are often defined in form of polynomials within the model for anode and cathode, respectively. For *OCP* definition, Colclasure et al. present an approach using ideal thermodynamic behavior extended by Redlich-Kister expansion:[19]

$$U = \frac{\Delta G^0}{F} + \frac{RT}{F} ln\left(\frac{1-\bar{c}}{\bar{c}}\right) + \frac{1}{F}\sum_{m=0}^{M_{RK}-1} A_m\left((2\bar{c}-1)^{m+1} - \left(\frac{2m\bar{c}(1-\bar{c})}{(2\bar{c}-1)^{1-m}}\right)\right) \quad [35]$$

with the standard-state chemical potential of an intercalated lithium relative to a lithium vacancy and lithium metal ΔG^0,[19] the number M_{RK} of Redlich-Kister coefficients A_m and $\bar{c}$ being the quotient of Li concentration at a certain state of charge c_c and maximum Li concentration c^{max}.

$$\bar{c} = \frac{c_c}{c^{max}} \quad [36]$$

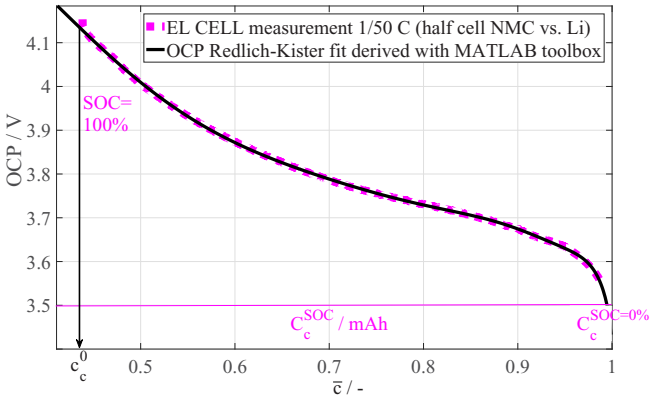

Figure 3. Fitting of model OCP polynomial with Redlich-Kister coefficients for NMC cathode based on EL Cell measurement.

For the anode, Redlich-Kister coefficients for graphite electrodes presented by Colclasure et al. were taken,[19] whereas for the NMC cathode according data was determined experimentally. Therefore a 1/50 C-Rate discharge in an EL CELL setup containing Li reference of the used NMC electrodes was performed and the respective half cell potential curve was taken for *OCP* curve definition.

After the measurement a Redlich-Kister fit was derived with the aid of MATLAB curve fitting toolbox (Figure 3). The potential at the begin of discharge when the cathode is fully charged (SOC=%100) was correlated to the initial concentration c^0_c for simulation. The derived Redlich-Kister coefficients are listed in Table I.

As described in Electronic and ionic conduction section, for the implementation of ionic conductivity κ a polynomial was used; the electrolyte diffusion coefficient D_e was then derived by the Nernst-Einstein relation. To achieve realistic electrolyte properties, for D_e a value was chosen which yielded best possible agreement between Nernst-Einstein relation and an ionic conductivity curve which was measured for the used electrolyte composition (EC:DEC 3:7, 1M $LiPF_6$) by Moosbauer.[24] A detailed description of this derivation is

Table I. Redlich-Kister fitting coefficients derived for NMC cathode based on EL-Cell OCP measurement.

coefficient	value
$\frac{\Delta G^0}{F}$	3.8 V
A_0	667.3
A_1	−40410
A_2	79720
A_3	−97760
A_4	46830
A_5	22990
A_6	−3107
A_7	−17430
A_8	−18180
A_9	−11280
A_{10}	−2092
A_{11}	5957
A_{12}	11220
A_{13}	13250
A_{14}	12220
A_{15}	8652
A_{16}	3140
A_{17}	−3662
A_{18}	−11130
$A_{19=(RK-1)}$	−18780

Table II. Parameters independent of calendering.

parameter	value	source
Lithium start concentration in solid (anode) $c_a^0(t=t_0)$ [mol m^{-3}]	$(0.99-0.1)\cdot c_a^{max}$	calculated
Lithium start concentration in solid (cathode) $c_c^0(t=t_0)$ [mol m^{-3}]	$0.44\cdot c_c^{max}$	calculated
Lithium max. concentration in solid (anode) c_a^{max} [mol m^{-3}]	28605	calculation
Lithium max. concentration in solid (cathode) c_c^{max} [mol m^{-3}]	50862	calculation
Lithium salt start concentration in liquid electrolyte $c_e^0(t=t_0)$ [mol m^{-3}]	1000	experimental conditions, 1 M $LiPF_6$
particle radius anode R_a [µm]	6.825	material data sheet (D50/2)
particle radius cathode R_c [µm]	6.40	material data sheet (D50/2)
electrode thickness anode δ_a [µm]	43.10	measurement
porosity anode ε_a [-]	0.5585	calculation
solid volume fraction anode ε_a^s [-]	0.3871	calculation
separator thickness δ_s [µm]	20.00	material data sheet
double layer capacitance anode C_a^{DL} [F m^{-2}]	0.2	13
double layer capacitance cathode C_c^{DL} [F m^{-2}]	0.2	13
solid diffusion coefficient anode D_a^s [m^2 s^{-1}]	$9.12\cdot10^{-15}$	25
solid diffusion coefficient cathode D_c^s [m^2 s^{-1}]	$3.0\cdot10^{-15}$	25
Li^+ transference number t_+ [−]	0.24	26
temperature T [K]	293	experimental conditions
oxidation transfer coefficient α_{ox} [-]	0.5	13
reduction transfer coefficient α_{red} [-]	0.5	13
effective electronic conductivity anode σ_a^{eff} [S m^{-1}]	0.1752	measurement
electrolyte diffusion coefficient D_e [m^2 s^{-1}]	$0.6832\cdot10^{-10}$	chosen
reaction rate constant anode k [m$^{2.5}$ mol$^{-0.5}$ s^{-1}]	$2\cdot10^{-11}$	chosen
reaction rate constant cathode k [m$^{2.5}$ mol$^{-0.5}$ s^{-1}]	$2\cdot10^{-11}$	chosen
tortuosity anode τ_a [-]	1.5	chosen
tortuosity separator τ_s [-]	1.5	chosen

given in the appendix. Table II lists all parameters, which are assumed to be not affected by calendering and therefore held constant during simulation-based analysis of calendering impacts.

Parameters dependent on calendering.—Cathode thickness and porosity are obviously affected by calendering due to compaction of particle-pore structures (Figure 4), whereas calendering impacts on other parameters are more complex. Transportation pathways of ions and electrons which are exemplarily indicated by curved arrows in Figure 4 are assumed to be not only influenced by particle-pore structures between NMC and electrolyte. They are also affected by the structure of pores within the carbon black - binder matrix for ionic transport and by NMC particle-to-carbon black particle connections for electronic transport. Consequently, structural formation can lead to calendering dependent performance changes[27] which in terms of model parameters is expressed by ionic and electronic conductivities being significantly different from bulk material properties. Therefore, when evaluating calendering impacts we expect effective conductivities κ_{eff}, σ_{eff}, which deviate from the respective bulk material conductivities.

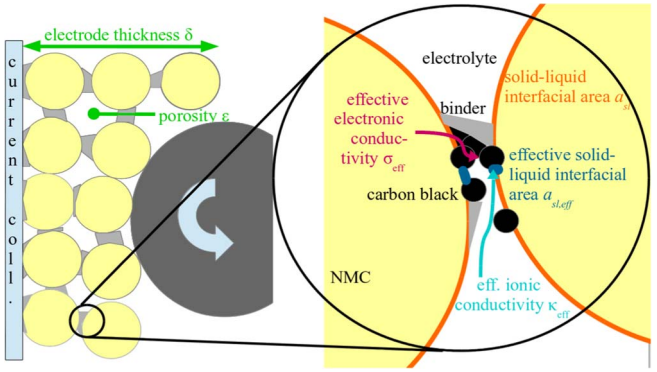

Figure 4. Illustration of parameters assumed to be affected in the cathode by calendering.

The same applies to solid-liquid interfacial area where theoretically the entire surface area of NMC particles a_{sl} may be used for the electrochemical reaction, allowing for low kinetic losses at 1 C-Rate discharge. However, it is assumed that a particular share of this surface area may not be electrochemically active, e.g. when contact to carbon black particles is insufficient and as such electron transport is hindered. Consequently, there is only a particular share of solid-liquid interfacial area effectively available for electrochemical reaction, which we denote by $a_{sl,eff}$. As calendering induced compaction leads to plastic deformation and thereby to a redistribution of the carbon black - binder matrix within the particle-pore network, an impact of effective solid-liquid interfacial area is expected. Within this work, cathode thickness and porosity were determined for non-calendered and 22%-calendered electrodes, the respective values are listed in Table III. For determination of tortuosities no experimental values were available, so identical values were chosen for both calendering conditions. In the lower separated section of Table III, the parameters are listed where calendering impacts are not at all or only with limitation measurable. Simulation values for these parameters were unknown and had to be determined by fitting electronic conductivities $\sigma_c^{0\%cal}$, $\sigma_c^{22\%cal}$, tortuosities $\tau_c^{0\%cal}$, $\tau_c^{22\%cal}$ and the introduced calendering dependent factors $\lambda_{asl}^{0\%cal}$ and $\lambda_{asl}^{22\%cal}$. A discussion based on the simulation results for tortuosity will be given in Results and discussion section, to evaluate if the assumption of identical tortuosities for both calendering cases is realistic.

Comparison between experimental and simulated discharge curves.—Based on the parameterization presented in the previous section, two parameter sets were derived, one for the cell containing a non-calendered cathode and another one for the cell containing a 22%-calendered cathode. Unknown parameters, being namely effective electronic conductivities $\sigma_{eff,c}^{0\%cal}$, $\sigma_{eff,c}^{22\%cal}$, effective ionic conductivities $\kappa_{eff,c}^{0\%cal}$, $\kappa_{eff,c}^{22\%cal}$ and effective solid-liquid interfacial areas $a_{eff,c}^{0\%cal}$, $a_{eff,c}^{22\%cal}$ were determined by fitting the respective electronic conductivities $\sigma_c^{0\%cal}$, $\sigma_c^{22\%cal}$, tortuosities $\tau_c^{0\%cal}$, $\tau_c^{22\%cal}$ and calendering dependent factors $\lambda_{asl}^{0\%cal}$ and $\lambda_{asl}^{22\%cal}$. A qualitative agreement between experimental and simulated discharge curves at various C-Rates for both calendering cases is shown in Figure 5. Slight deviations may results

Table III. Parameters dependent on calendering.

parameter	value	source
electrode thickness cathode $\delta_c^{0\%cal}$ [µm]	61.36	measurement
electrode thickness cathode (22% calendered) $\delta_c^{22\%cal}$ [µm]	48.95	measurement
porosity cathode (non-calendered) $\varepsilon_c^{0\%cal}$ [-]	0.6259	calculation
porosity cathode (22% calendered) $\varepsilon_c^{22\%cal}$ [-]	0.5311	calculation
solid volume fraction cathode (non-calendered) $\varepsilon_s^{0\%cal}$ [-]	0.3040	calculation
solid volume fraction cathode (22% calendered) $\varepsilon_s^{22\%cal}$ [-]	0.3810	calculation
tortuosity cathode (non-calendered) $\varepsilon_s^{0\%cal}$ [-]	1.5	chosen
tortuosity (22% calendered) $\varepsilon_s^{22\%cal}$ [-]	1.5	chosen
effective electronic conductivity cathode (non-calendered) $\sigma_{eff,c}^{0\%cal}$ [S m^{-1}]	0.0005	fit of $\sigma_c^{0\%cal}$
effective electronic conductivity cathode (22% calendered) $\sigma_{eff,c}^{22\%cal}$ [S m^{-1}]	0.0015	fit of $\sigma_c^{22\%cal}$
effective ionic conductivity (cathode non-calendered) $\kappa_{eff}^{0\%cal}$ [S m^{-1}]	$\frac{\kappa \cdot 0.6259}{1.5}$	fit of $\tau_c^{0\%cal}$
effective ionic conductivity (cathode 22% calendered) $\kappa_{eff}^{22\%cal}$ [S m^{-1}]	$\frac{\kappa \cdot 0.5311}{1.5}$	fit of $\tau_c^{22\%cal}$
effective solid-liquid interfacial area (non-calendered) $a_{sl,eff}^{0\%cal}$ [m^2 m^{-3}]	$\frac{3 \cdot \varepsilon_s}{R_p} \cdot 0.12$	fit of $\lambda_{asl}^{0\%cal}$
effective solid-liquid interfacial area (22% calendered) $a_{sl,eff}^{22\%cal}$ [m^2 m^{-3}]	$\frac{3 \cdot \varepsilon_s}{R_p} \cdot 1.0$	fit of $\lambda_{asl}^{22\%cal}$

from simplifying model assumptions, e.g. that diffusion constants are not affected by Li concentrations or that particle radii and electrode thicknesses do not account for statistical variations within ranges of production tolerances. Comparison of Figures 5a and 5b shows that the cell containing non-calendered cathodes performed worse than the one assembled with 22%-calendered cathodes. This performance loss increases with C-Rates which makes relatively high C-Rates most informative for investigation of parameter impacts between both cases. However, at 2 C losses in the non-calendered electrode are so high that voltage dropped immediately after current was drawn, delivering hardly any discharge capacity. Therefore for further simulation based investigation we focus on 1 C discharge curves.

Results and Discussion

Electrochemical and electrical characterization of calendering impacts.—Determination of cell capacities from formation shows only a slight impact of calendering: $C^{0\%\text{cal}} = 31.74$ mAh versus $C^{22\%\text{cal}} = 32.06$ mAh. However, the deviations are only negligibly small at the relatively low formation discharge currents (0.05 C). For battery operation at 1 C, non-calendered cathodes caused performance losses, compared to 22%-calendered ones. As such, overpotentials were significantly reduced by a 22% cathode calendering (Figure 6).

Effective electronic conductivities of dry electrode samples were measured as described in Thicknesses and electronic conductivities of electrodes section. For the non-calendered cathodes a mean value of $\sigma_{exp}^{0\%\text{cal}} = 0.0052 \pm 0.0003$ S/m (5 samples) was measured. The 22%-calendered cathodes showed an enhanced electronic conductivity with $\sigma_{exp}^{22\%\text{cal}} = 0.0069 \pm 0.0004$ S/m (5 samples). Accordingly, it can be stated that calendering improved the electronic conductivity of the investigated cathodes.

The performed experiments show that there is a significant calendering impact on effective electronic conductivity. However, it is doubtful if measured conductivity values of the dry electrode samples under 40 N compression force which was applied in the experimental setup, is identical to the conductivities under full cell assembly conditions with electrolyte, which causes surface changes such as the solid electrolyte interphase. Furthermore it is to be examined, how much the calendering impacts on other parameters contribute to observed performance losses. Therefore, simulation supported analysis is presented in the following subsections.

Evaluation of parameter fitting.—Calendering dependent geometry parameters for simulation were taken from Table III, whereas other parameters were assumed to be not reliably measurable so that respective values for electronic conductivity σ, tortuosity τ and the calendering dependent factor λ_{asl} were fitted so that agreement between experimental and simulated discharge curves was achieved, the resulting values are listed in Table IV. Physically these values also imply that effective ionic conductivity κ_{eff} is only affected by calendering in the way that porosity ε is decreased. However, tortuosity τ is not increased significantly by 22%-calendering. One possible reason is that 22% of calendering induced compaction is not enough to cause tortuosity effects on the effective ionic conductivity. Another possible

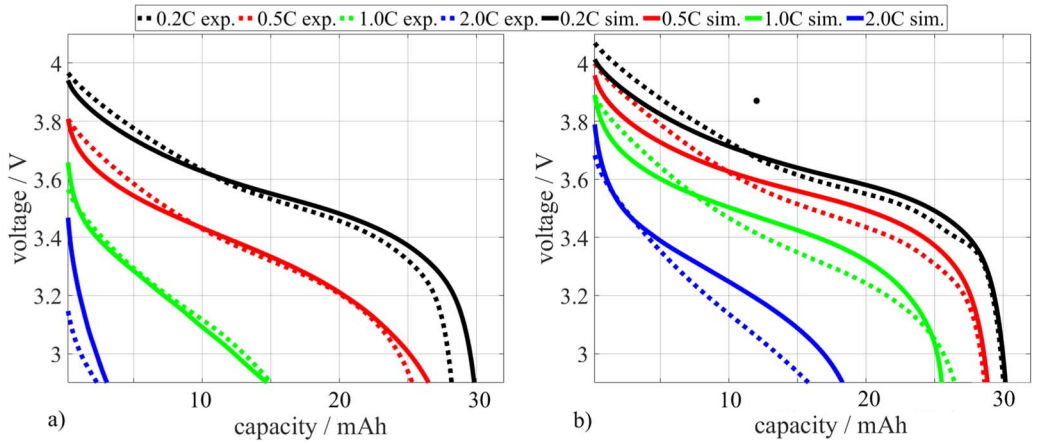

Figure 5. Experimental (dashed lines) and simulated (solid lines) C-Rate test for a) cells containing non-calendered and b) cells containing 22%-calendered cathodes.

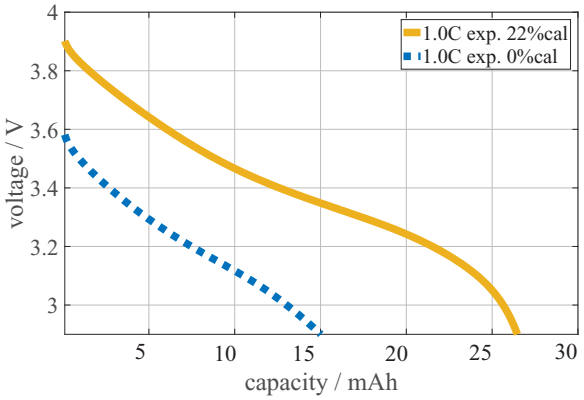

Figure 6. Discharge curves at 1 C-Rate of pouch full cells containing non-calendered (dashed line) and 22%-calendered (solid line) cathodes respectively.

reason is that the tortuosity may actually have changed but, as the ionic transport is not limiting it does not cause performance losses. Effective electronic conductivity σ_{eff} and effective solid-liquid interfacial area $a_{sl,eff}$ are increased by calendering. In the case of interfacial area, $\lambda_{asl}^{0\%cal} = 0.12$ suggests that in a non-calendered cathode only 12% of the theoretically available interfacial area a_{sl} can be utilized for electrochemical reaction, whereas in the 22%-calendered case no limitation occurs so that 100 % of a_{sl} can be utilized.

It is particularly interesting to discuss simulated values for effective electronic conductivities $\sigma_{eff}^{0\%cal} = 0.0005$ S/m, $\sigma_{eff}^{22\%cal} = 0.0015$ S/m and to compare them to the measured ones $\sigma_{exp}^{0\%cal} = 0.0052$ S/m, $\sigma_{exp}^{22\%cal} = 0.0069$ S/m introduced in Electrochemical and electrical characterization of calendering impacts section. Effective electronic conductivities are worse in the non-calendered cathode than in the 22%-calendered one in both, simulation and measurement. However, absolute values are significantly lower in the simulation and also the difference between both calendering states turns out to be larger in simulation. Simulation based analysis yields that the effective electronic conductivity in non-calendered cathodes is only 33% of that found in 22%-calendered ones, whereas due to experimental investigation it was assumed to be 75%. Reasons for the higher conductivities determined experimentally may be first that dry samples were taken and second that the 40 N compression force of the experimental setup additionally increased conductivities of the samples compared to the unpressurized conditions inside a full cell, filled with electrolyte which is considered by simulation. Especially the compression force may be a reason considering that in the measurement the effective electronic conductivity of non-calendered cathodes was increased to 75 % of the respective value for the 22%-calendered one.

Uniqueness of parameter fitting.—Impacts of the particular fitting parameters on the shape of discharge curves, on voltage and discharge capacities at various C-Rates are different from each others. This is analyzed by comparing the experimentally observed calendering impact on discharge curves to the impacts of the three fitting parameters separately; corresponding parameter sets are listed in Table V. in cases a) - c) where only one fitting parameter was adjusted respectively to achieve the described performance losses, the unchanged parameters are the values derived for the 22%-calendered case. The comparison described above is shown in Figure 7a for the case where only the tortuosity which affects the effective ionic conductivity is decreased in the model. For simulation of 0.2 C and 0.5 C discharge, a qualitative agreement with experimental curves can be achieved. However, at 1 C and 2 C the voltages at the begin of discharge are overestimated and furthermore simulated curves deviate significantly from experiments as a limitation by effective ionic conductivity appears to cause a steeper slope. Figure 7b shows curves based on the assumption that the electronic conductivity is the only fitting parameter to describe performance losses in non-calendered cathodes. It can be observed that the shape of the experimental curves cannot be reproduced as the simulated curves show a rather linear slope, especially visible at C-Rates $\geq$ 0.5 C. On the contrary, considering the calendering dependent factor affecting the effective solid-liquid interfacial area as the only fitting parameter, characteristic performance losses appear rather in form of a parallel downwards shift of the discharge curves leading to a deviation from experimental curves by a too gentle slope (Figure 7c). These simulations show that the real calendering induced performance losses can only consist of a combination of several fitting parameter impacts. Regarding the uniqueness of simulation results, further limitations can be derived by physically realistic assumptions. A solution which can be excluded in general and therefore is not relevant for simulation, is the explanation of performance losses by deterioration of effective ionic conductivity κ_{eff}. As explained by Thorat et al.[12] tortuosity would be expected to be lower in non-calendered electrodes due to their higher porosity which should improve rather than decrease κ_{eff}. Therefore the only parameters which are reasonable to cause the observed performance losses are the effective electronic conductivity σ_{eff} and the effective solid-liquid interfacial area $a_{sl,eff}$. In comparison to the solution presented in Evaluation of parameter fitting section, an alternative scenario was simulated which assumes that the impact of $a_{sl,eff}$ on performance is increased, where the respective parameter sets are listed in Table Vd). This case shows that an agreement of a quality which is only slightly worse than for the solution discussed in Evaluation of parameter fitting section. (Figure 7d) However, with λ_{asl}=0.01 this alternative would imply an effective solid-liquid interfacial area of only 1% which appears unrealistically low, therefore the parameter set presented in Evaluation of parameter fitting section was chosen.

Table IV. Resulting values from parameter fitting.

parameter	0%-calendered	22%-calendered
tortuosity τ [-]	1.5	1.5
electronic conductivity σ [S/m]	0.0017	0.0040
factor affecting effective solid-liquid interfacial area λ_{asl} [-]	0.12	1.00

Analysis of particular parameter impacts.—As shown in Table VI, five parameter configurations were defined for analysis purposes, where state 1 and 5 denote the 22%-calendered and non-calendered case, respectively. Intermediate states (2–4) were formulated to evaluate the single parameter contributions on discharge curves. Between each step, i.e. transition from one to the next state,

Table V. Alternative parameter sets for discussion of uniqueness, corresponding to Figure 7, including the cases of performance losses caused only by reduction of tortuosity a), only by reduction of electronic conductivity b), only by reduction of the factor affecting effective solid-liquid interfacial area c), by an alternative parameter combination where the effective solid-liquid interfacial area has a higher impact d) than in the parameter set chosen as more realistic for simulation in Evaluation of parameter fitting section (r).

parameter	a)	b)	c)	d)	(r)
tortuosity τ [-]	15	1.5	1.5	1.5	1.5
electronic conductivity σ [S/m]	0.004	0.001	0.004	0.0024	0.0017
factor affecting effective solid-liquid interfacial area λ_{asl} [-]	1.0	1.0	0.001	0.01	0.12

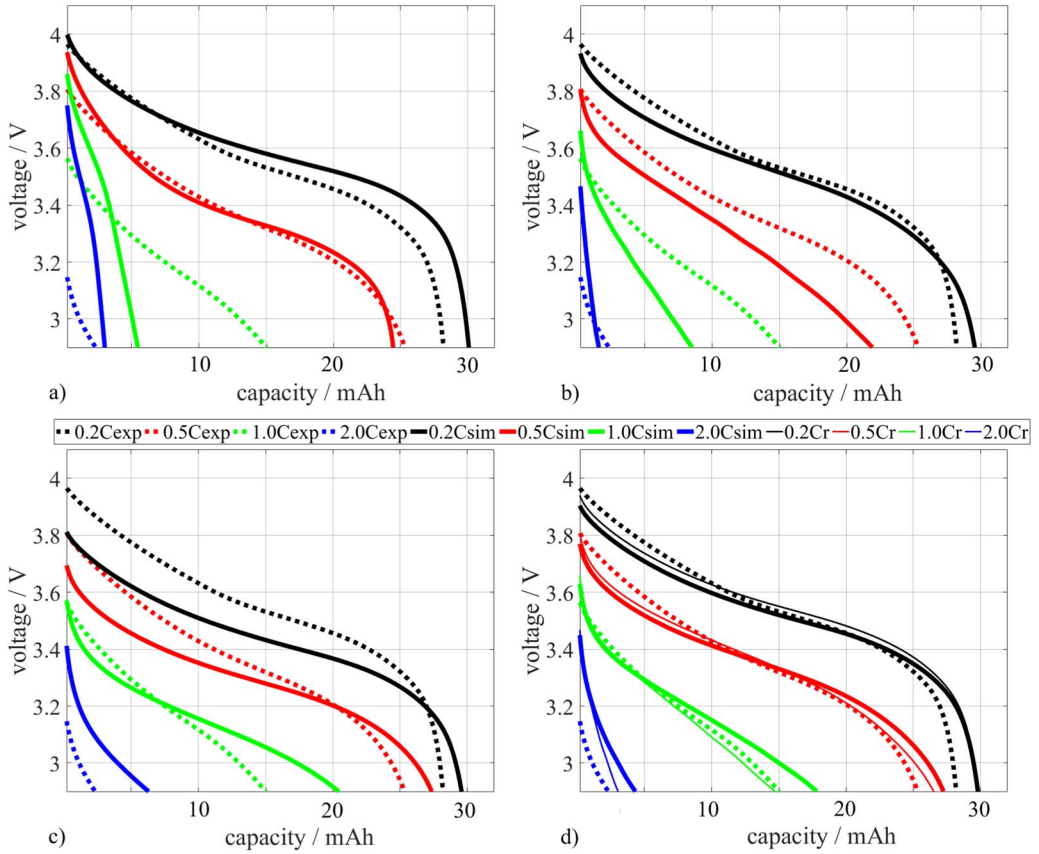

Figure 7. Simulation of performance losses in non-calendered cathodes based on deterioration of a) effective ionic conductivity, b) effective electronic conductivity, c) effective solid-liquid interfacial area and d) alternative parameter set where thin lines show as a reference (r) curves simulated with the parameter set presented in Evaluation of parameter fitting section.

only one parameter was changed, respectively. Variations of cathode thickness δ_c and porosity ε_c, denoted as $\Delta_{\delta+\varepsilon}$ were merged in the first step accounting for compaction of geometry. Impacts on the other parameters, being namely effective electronic conductivity σ_{eff}, effective ionic conductivity κ_{eff} and effective solid-liquid interfacial area $a_{sl,eff}$ were simulated by variations of electronic conductivity, Δ_σ, variations of tortuosity Δ_τ and previously introduced calendering dependent factor λ_{asl}, i.e. $\Delta_{\lambda_{asl}}$. Simulation results of the particular parameter impacts from state 1 to 5 on discharge performance are shown in Figure 8. State 1 which represents a 22%-calendered cathode, is taken as reference for analysis because it represents a well functioning cell. The performance loss which was observed in the non-calendered case appears to be a superposition of the particular parameter impacts. The first fraction of performance losses is caused by larger thickness and porosity of the non-calendered cathode. It can be seen in Figure 8 that the geometric compaction only contributes a relatively small share of the overpotential difference between cells containing a 22%-calendered cathode and ones being assembled with a non-calendered cathode; furthermore the geometric impact does not lead to a loss of discharge capacity. This shows the importance of simulation-supported analysis because the parameters contributing most are obviously not the geometric ones, which can be evaluated by experimental methods only. Nevertheless, overpotentials by compaction are not negligible; to understand the correlation between geometric impact and overpotentials, $LiPF_6$ transport within the electrolyte for both geometry cases was analyzed. Figure 9 shows the respective $LiPF_6$ concentration profiles along the cathode length normalized to the thickness of the non-calendered cathode $\overline{x}_c = \frac{x_c}{\delta_c^{0\%cal}}$ which implies that the non-calendered electrode ends at $\overline{x}_c$=1, whereas the thinner, 22%-calendered one only reaches about $\overline{x}_c$=0.76. The $LiPF_6$ concentration curves were simulated at SOC=50% which corresponds to points on the respective discharge curves in Figure 8 at capacity of about 12.5 mAh where the investigated overpotentials occur; an analysis e.g. at SOC=0% which corresponds to a discharge capacity of about 25 mAh, would be not reasonable because both curves reach the lower cutoff voltage in that point and converge as only small losses of discharge capacity occur. $LiPF_6$ concentration in Figure 9 is lower for the 22%-calendered case in general because the compacted electrode contains less electrolyte than the non-calendered one.

However, this is not relevant for performance analysis. Instead, the overpotentials are caused by various differences of $LiPF_6$

Table VI. List of simulation parameter configurations.

state	description	geometry	ionic cond.	el. cond.	sol.-liq.
1	22%-calendered	$\delta_c^{22\%cal}$, $\varepsilon_c^{22\%cal}$	$\tau^{22\%cal}$	$\sigma^{22\%cal}$	$\lambda_{asl}^{22\%cal}$
2	state 1 + $\Delta_{\delta+\varepsilon}$	$\delta_c^{0\%cal}$, $\varepsilon_c^{0\%cal}$	$\tau^{22\%cal}$	$\sigma^{22\%cal}$	$\lambda_{asl}^{22\%cal}$
3	s2 + Δ_τ	$\delta_c^{0\%cal}$, $\varepsilon_c^{0\%cal}$	$\tau^{0\%cal}$	$\sigma^{22\%cal}$	$\lambda_{asl}^{22\%cal}$
4	s3 + Δ_σ	$\delta_c^{0\%cal}$, $\varepsilon_c^{0\%cal}$	$\tau^{0\%cal}$	$\sigma^{0\%cal}$	$\lambda_{asl}^{22\%cal}$
5	non-calendered (s4 + $\Delta_{\lambda_{asl}}$)	$\delta_c^{0\%cal}$, $\varepsilon_c^{0\%cal}$	$\tau^{0\%cal}$	$\sigma^{0\%cal}$	$\lambda_{asl}^{0\%cal}$

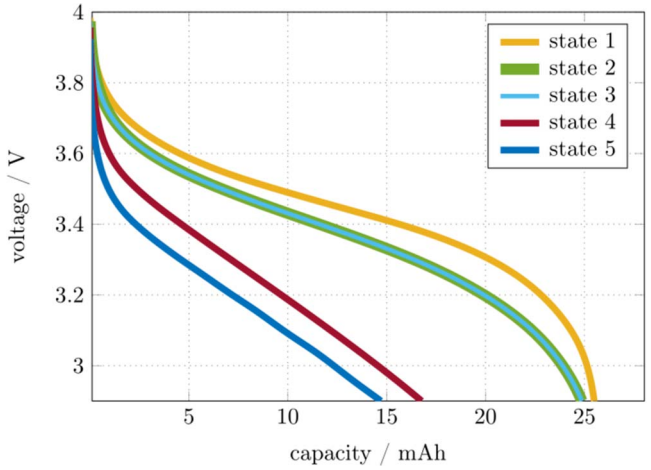

Figure 8. Particular calendering dependent parameter impacts on discharge curves at 1 C.

concentrations along the cathode length between separator and current collector for the distinct calendering cases respectively:

$$\left[c_e^{0\%cal}(\bar{x}_c = 0) - c_e^{0\%cal}(1)\right. \quad - \left[c_e^{22\%cal}(0) - c_e^{22\%cal}(0.76)\right.$$

$$= 215 - 199 = 16\frac{mol}{m^3} \qquad [37]$$

Substitution of the result of Equation 37, in form of c_e into Equation 17 and solving for the potential gradient $\frac{\partial \phi_e}{\partial x}$ yields the overpotentials $\eta \approx 0.07$ V shown in Figure 8 between state 1 and 2 at a capacity of 12.5 mAh. Within the range of calendering between 0% and 22%, effective ionic conductivity is not significantly affected by calendering which leads to states 2 and 3 showing the same performances in Figure 8. The largest fraction of performance loss is found for transition between states 3 and 4, which is caused by worse effective electronic conductivity of non-calendered cathodes. A detailed discussion of correlations between the parameter impact and the cell internal Li transport will be given below. The third fraction of performance loss is caused by changes in the effective solid-liquid interfacial area. It is smaller in non-calendered cathodes. This loss is physically reasoned as a decrease of effective interfacial area reduces the volume rate of Li^+ exchange current generation j^{Li} in Equation 24. When analyzing the dominant impact of worse electronic conductivity in non-calendered cathodes by simulation of Li concentration profiles

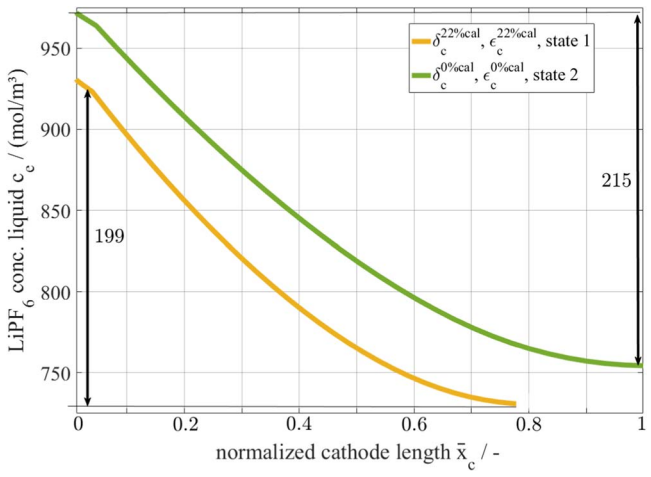

Figure 9. Differences of $LiPF_6$ concentrations between separator ($\bar{x}_c$=0) and current collector ($\bar{x}_c$=1) for the non-calendered and for the 22-% calendered (current collector at $\bar{x}_c$=0.76) cathode geometry.

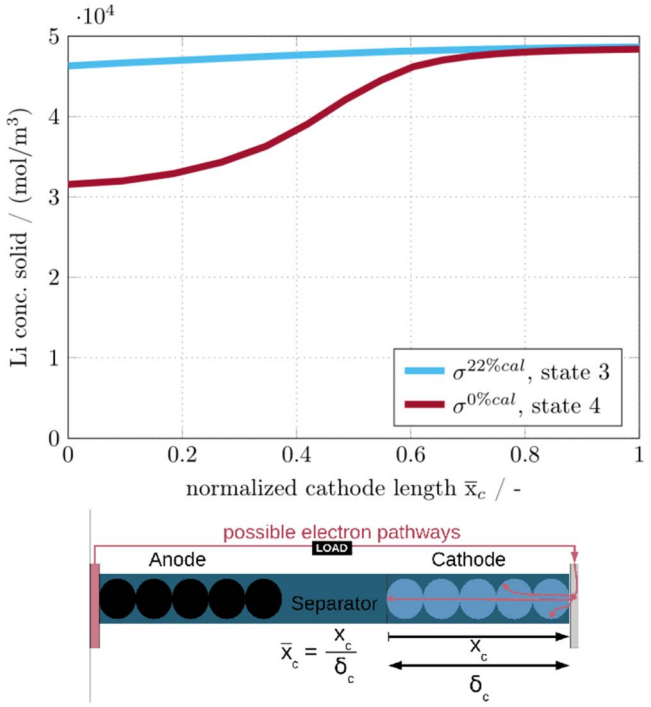

Figure 10. Li solid concentration profiles at the surfaces of particles and $t(SOC = 0\%)$; worse electronic conductivity in non-calendered cathode leads to a reduction of Li intercalation close to separator where electrons have the longest pathway to be supplied to.

on the surfaces of solid active material particles (r=R_p) at the end of discharge ($t(SOC = 0\%)$), it becomes obvious that Li intercalation is reduced close to the separator, $\bar{x}_c = 0$ (Figure 10) to about $3.1 \cdot 10^4$ mol/m³ whereas the respective value for state 3 is about $4.7 \cdot 10^4$ mol/m³. This reduction arises as transport of electrons over the relatively long distance between separator and current collector becomes limiting so that overpotentials close to the separator increase. Electrons cannot be supplied fast enough at this critical location to keep the local intercalation process constant at 1 C. In this case for analysis, SOC=0% was chosen which in Figure 8 corresponds to discharge capacities of about 25 mAh for state 3 and 16.5 mAh for state 4; on these points not only overpotentials but also discharge capacity loss due to worse effective electronic conductivity is maximal.

As a final result, simulation supported analysis has shown that for the cells discussed here, calendering is necessary to prevent significant performance losses at C-Rates equal or higher than 1 C. The most limiting parameter is the effective electronic conductivity which can be enhanced by calendering. To achieve further improvement of performance, one option would be to increase calendering strength to values higher than 22%. Within the calendering ranges investigated in this study no significant effect on effective ionic conductivity was observed. However, it has to be assumed that for higher calendering strength than 22%, tortuosity effects will appear due to narrowing of pores, so that at a certain calendering strength effective ionic conductivity may become limiting. Another option to improve performance would be to add more than 4 mass-% of carbon black to increase effective electronic conductivity. It would also be reasonable to perform further studies to evaluate combinations of both options in order to define an optimal calendering strength and an optimal carbon black content.

Conclusions

Impacts of electrode calendering on battery performance are commonly investigated either experimentally or by simulation. In this study an approach is presented which combines experimental and

theoretical methods. For the experimental part, cells with two different cathode calendering configurations were manufactured. Experimental investigations showed that the cells containing non-calendered cathodes performed significantly worse than the ones which were assembled with 22%-calendered cathodes. To analyze the underlying physical impacts on cell internal processes, a P2D model was parameterized for each configuration. After model validation, impacts of the particular calendering dependent parameters on battery performance were simulatively investigated. It was shown that within the calendering variation range between 0% and 22%, effective ionic conductivity is only affected due to porosity change, no significant tortuosity effects could be identified. The larger thickness and porosity of non-calendered cathodes caused performance losses in the form of overpotentials; available discharge capacity was not deteriorated, though. Effective electronic conductivity was shown to be worse in non-calendered cathodes which caused the dominant share of performance losses. This impact caused not only overpotentials but also a decrease of discharge capacity. These losses arise close to the boundary of cathode and separator, where the conduction distance of electrons is farthest as they are supplied at the current collector side and have to be transported across the entire cathode. Another fraction of performance losses in non-calendered cathodes was induced by a reduction of effective solid-liquid interfacial area available for electrochemical reaction. The results of this study imply that a combination of increasing calendering strength of cathodes beyond 22% and applying higher carbon black contents than 4 mass-% is promising in order to achieve further improvements of battery performance.

Acknowledgments

Thanks for financial funding to the German Federal Ministry of Education and Research and to the German Federal Ministry for Economic Affairs and Energy. Thanks for technical support to the Institute of Environmental and Sustainable Chemistry, TU Braunschweig.

Appendix: Discussion on the Parameterization of Electrolyte Diffusivity

To determine an appropriate electrolyte diffusion coefficient D_e the Nernst-Einstein relation was used applying the formulae:

$$\kappa^e_{\mathrm{NER}} = \frac{\varepsilon}{\tau} \cdot c_e(x) \cdot \frac{F^2 \cdot (D_+ + D_-)}{RT} \quad [A1]$$

$$D_e = \frac{2D_+D_-}{D_+ + D_-} \quad [A2]$$

and

$$t_+ = \frac{D_+}{D_+ + D_-} \quad [A3]$$

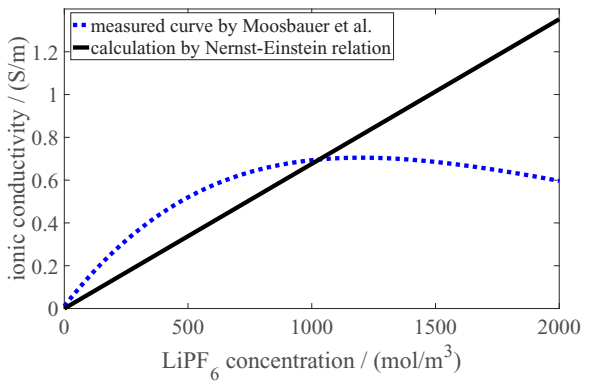

Figure A1. Comparison of ionic conductivities between measurement and calculation with $D_e = 0.6832 \cdot 10^{-10}$ m^2/s.

Table A1. Fitting parameters derived for the polynomial to describe the ionic conductivity of 3:7 EC:DEC, 1 M $LiPF_6$ electrolyte.

coefficient	value
B_0	-2.68462
B_1	0.01668
B_2	-0.01073
B_3	$-2.46 \cdot 10^{-5}$
B_4	$-1.86 \cdot 10^{-5}$
B_5	$1.32 \cdot 10^{-5}$
B_6	$3.46 \cdot 10^{-7}$
B_7	$-7.68 \cdot 10^{-8}$
B_8	$-1.04 \cdot 10^{-10}$
B_9	$-1.02 \cdot 10^{-11}$
B_{10}	$1.07 \cdot 10^{-11}$
B_{11}	$-3.51 \cdot 10^{-13}$

as given by Newman et al.[20] the diffusion coefficients of cations D_+ and anions D_- can be written as:

$$D_+ = \frac{D_e}{2 - 2t_+} \quad [A4]$$

and

$$D_- = \frac{D_e}{2t_+} \quad [A5]$$

with the Li^+ transference number t_+. The calculation of Equation A1 results in an alternative description of effective ionic conductivity κ^e_{NER} according to the Nernst-Einstein relation in form of a straight line and realizes with $D_e = 0.6832 \cdot 10^{-10}$ m^2/s an acceptable agreement with the curve from Moosbauer[24] in the range of $LiPF_6$ concentrations $\leq$ 1000 mol/m^3 (Figure A1). This range is relevant for the cathode and investigations of calendering impacts focused in this study. Equation A1 was not used in the model equations but only applied to determine D_e which would have to be measured otherwise. The Nernst-Einstein relation is a useful tool for parameterization as ionic conductivity and the electrolyte diffusion coefficient are coupled mathematically. As mentioned in section Electronic and ionic conduction the fitting coefficients $B_0 - B_{11}$ of Equation 20 are listed in Table A1.

List of Symbols

A	geometric area, m^2
a_{sl}	solid-liquid interfacial area, m^2 m^{-3}
c	concentration, mol m^{-3},
C	capacity, Ah,
C_{DL}	double layer capacitance, F m-2
D	diffusion coefficient, m^2 s^{-1}
E	voltage, V
F	Faraday's constant, 96485 C mol^{-1}
I	current, A
j^{DL}	volume rate of double layer current generation A m^{-3}
j^{Li}	volume rate of Li^+ current generation A m^{-3}
j_0	exchange current density A m^{-2}
J	current density A m^{-2}
k	reaction rate constant, m$^{2.5}$ mol$^{-0.5}$ s^{-1}
L	length, m
M	molar mass, g mol^{-1}
M_{RK}	number of Redlich-Kister coefficients, g mol^{-1}
n	amount of substance, mol
r	radial coordinate, -
R_Ω	electronic resistance, Ω
R	ideal gas constant, 8.314 J mol^{-1} K^{-1}
R_p	particle radius, m
SOC	state of charge, -
t_+	Li^+ transference number, -
T	temperature, K
U	open circuit potential, V
V	volume, m^3
x	spacial coordinate

Greek

α	transfer coefficient, -
δ	electrode thickness, m
ε	volume fraction (porosity), -
ε_s	volume fraction of solid component, -
λ_{asl}	calendering dependent factor for effective solid-liquid interfacial area, -
η	overpotential, V
κ	ionic conductivity S m^{-1}
η	overpotential, V
ρ	density, g m^3
σ	electronic conductivity, S m^{-1}
τ	tortuosity, -
ϕ	electric potential, V
ϖ	electrode material loading, g m^{-2}
ζ	mass fraction, -

Subscripts and Superscripts

a	anode
c	cathode
cal	calendered
DL	double layer
e	electrolyte
eff	effective
exp	experimental (measured)
Li	Lithium
max	maximum
NER	derived by Nernst-Einstein relation
s	solid
0	initial
$+$	cation
$-$	anion

References

1. W. Haselrieder, S. Ivanov, D. K. Christen, H. Bockholt, and A. Kwade, *ECS Trans.*, **50**(26), 59 (2013).
2. H. Zheng, G. Liu, X. Song, and V. Battaglia, *ECS Trans.*, **11**(32), 1 (2008).
3. H. Zheng, L. Tan, G. Liu, X. Song, and V. S. Battaglia, *Journal of Power Sources*, **208**, 52 (2012).
4. G.-F. Yang and S.-K. Joo, *Electrochimica Acta*, **170**, 263 (2015).
5. A. van Bommel and R. Divigalpitiya, *Journal of The Electrochemical Society*, **159**(11), A1791 (2012).
6. N. Loeffler, J. von Zamory, N. Laszczynski, I. Doberdo, and G.-T. Kim, *Journal of Power Sources*, **248**, 915 (2014).
7. V. Srinivasan and J. Newman, *Journal of The Electrochemical Society*, **151**(10), A1530 (2004).
8. J. Ott, B. Völker, Y. Gan, R. M. McMeeking, and M. Kamlah, *Acta Mechanica Sinica*, **29**(5), 682 (2013).
9. E. Martinez-Rosas, R. Vasquez-Medrano, and A. Flores-Tlacuahuac, *Computers and Chemical Engineering*, **35**, 1937 (2011).
10. G. Gaiselmann, M. Neumann, O. Pecho, T. Hocker, V. Schmidt, and L. Holzer, *AlChE Journal*, **60**(6), 1983 (2014).
11. B. Vijayaraghavan, D. R. Ely, Y.-M. Chiang, R. Garcia-Garcia, and R. E. Garcia, *Journal of The Electrochemical Society*, **159**(5), A548 (2012).
12. I. V. Thorat, D. E. Stephenson, N. A. Zacharias, K. Zaghib, J. N. Harb, and D. R. Wheeler, *Journal of Power Sources*, **188**, 592 (2009).
13. N. Legrand, S. Raël, B. Knosp, M. Hinaje, P. Desprez, and F. Lapicque, *Journal of Power Sources*, **251**, 370 (2014).
14. W. Fang, O. J. Kwon, and C. Y. Wang, *International Journal of Energy Research*, **34**, 107 (2009).
15. J. Newman and W. Tiedemann, *AlChE Journal*, **21**(1), 25 (1975).
16. M. Doyle, T. F. Fuller, and J. Newman, *Journal of The Electrochemical Society*, **140**, 1526 (1993).
17. M. Ecker, T. K. D. Tran, P. Dechent, S. Käbitz, A. Warnecke, and D. U. Sauer, *Journal of The Electrochemical Society*, **162**(9), A1836 (2015).
18. M. Ecker, S. Käbitz, I. Laresgoiti, and D. U. Sauer, *Journal of The Electrochemical Society*, **162**(9), A1849 (2015).
19. A. M. Colclasure and R. J. Kee, *Electrochimica Acta*, **55**, 8960 (2010).
20. J. Newman and K. E. Thomas-Alyea, *Electrochemical Systems*, 297, John Wiley & Sons, Hoboken New Jersey (2004).
21. H. Yoshizawa and T. Ohzuku, *Journal of Power Sources*, **174**, 813 (2007).
22. W. Haselrieder, S. Ivanov, H. Y. Tran, S. Theil, L. Froböse, B. Westphal, M. Wohlfahrt-Mehrens, and A. Kwade, *Progress in Solid State Chemistry*, **42**, 157 (2014).
23. C. Wurm, O. Öttinger, S. Wittkämper, R. Zauter, and K. Vuorilehto, *Handbuch Lithium-Ionen-Batterien*, 49, Springer, Berlin Heidelberg (2013).
24. D. J. Moosbauer, *Elektrochemische Charakterisierung von Elektrolyten und Elektroden für Lithium-Ionen-Batterien*, Dissertation, Universität Regensburg (2010).
25. M. Park, X. Zhang, M. Chung, G. B. Less, and A. M. Sastry, *Journal of Power Sources*, **195**, 7904 (2010).
26. S. Zugmann, M. Fleischmann, M. Amereller, R. M. Gschwind, M. Winter, and H. J. Gores, *Journal of Chemical and Engineering Data*, **56**, 4786 (2011).
27. H. Bockholt, W. Haselrieder, and A. Kwade, *Powder Technology*, **297**, 266 (2016).
28. P. Arora and R. E. White, *Journal of The Electrochemical Society*, **145**(10), 3647 (1998).